Number-phase Wigner representation for scalable stochastic simulations of controlled quantum systems

M. R. Hush,[1] A. R. R. Carvalho,[2] and J. J. Hope[1]

[1]*Department of Quantum Science, Research School of Physics and Engineering, The Australian National University, ACT 0200, Australia*

[2]*Centre for Quantum Computation and Communication Technology, Department of Quantum Sciences, Research School of Physics and Engineering, The Australian National University, Canberra, ACT 0200, Australia*

(Received 30 May 2011; revised manuscript received 30 September 2011; published 7 February 2012)

Simulation of conditional master equations is important to describe systems under continuous measurement and for the design of control strategies in quantum systems. For large bosonic systems, such as Bose-Einstein condensates and atom lasers, full quantum-field simulations must rely on scalable stochastic methods. Currently, these methods have a convergence time that is restricted by the use of representations based on coherent states. Here, we show that typical measurements on atom-optical systems have a common form that allows for an efficient simulation using the number-phase Wigner (NPW) phase-space representation. We demonstrate that a stochastic method based on the NPW can converge orders of magnitude longer and more precisely than its coherent equivalent. We then examine how these methods can be used in multimode simulations, demonstrated by a simulation of a two-mode Bose-Hubbard model. Finally, we combine these techniques to demonstrate a full-field simulation of a realistic multimode quantum system controlled by active feedback.

DOI: 10.1103/PhysRevA.85.023607 PACS number(s): 42.50.Lc, 03.75.Gg, 03.75.Kk, 05.10.Gg

I. INTRODUCTION

Exciting advances in physics have led to a boom of research into technologies that exploit fundamental quantum properties. Such quantum technologies now encompass more than lasers and superconductors. Indeed, there are applications for precision metrology [1,2], quantum-information processing, and quantum cryptography [3,4]. A key feature of quantum technologies is that they require the precise creation, measurement, and control of individual quantum systems. In particular, measurement-based feedback control has shown promise as an effective and robust technique for controlling quantum systems. The first experiments [5–8] and many theoretical papers [9–16] on feedback control of quantum systems have been applied to relatively low-dimensional systems. This paper describes a technique for efficient simulation of large bosonic conditional quantum systems that is orders of magnitude more precise and converges for significantly longer time scales than previous methods and that scales logarithmically with the size of the Hilbert space.

A large bosonic system of particular interest to quantum science is the Bose-Einstein condensate (BEC). Measurement-based feedback control of BECs and atom lasers was first investigated in a single-mode model where a continuous number measurement was used to reduce the interaction-induced phase diffusion that limits the single-mode atom laser linewidth [17]. Then, it was shown that position measurement and feedback on a single trapped atom could bring it to the ground state [12,13], but the proposed measurement scheme was not suitable for large atomic clouds, such as a condensate. A multimode quantum-field model of a condensate measured by an existing experimental technique (phase-contrast imaging) then was produced, but it could only be solved using a semiclassical approximation [14,15]. Analysis of the linewidth of a multimode atom laser undergoing feedback requires a viable stochastic method for conditional quantum states that can deal with both high nonlinearities and numberlike measurements. This paper develops a method that fulfills both of these requirements.

The most effective methods for dynamic simulation of high-dimensional bosonic quantum systems are stochastic techniques based on phase-space representations [18,19]. Each stochastic method is derived from a specific phase-space representation, which is akin to the choice of a basis for the Hilbert space. Naively, these techniques require memory and computational resources that scale logarithmically with the size of the Hilbert space. Practically, the overall computational efficiency is system dependent and strongly depends on how well the underlying phase-space representation matches the natural basis for the state of the quantum system under consideration. The most commonly used stochastic simulation methods are based on phase-space representations that use Gaussian states. These methods have enabled the simulation of quantum-optical [19,20], atomic [17,21,22], and fermionic quantum fields [23]. In particular, stochastic methods have been used extensively in the field of quantum-atom optics where dilute atomic gases can be cooled to produce BECs and atom lasers [24–26]. The two most successful varieties are based on the positive-P and the truncated Wigner (TW) representations. The positive-P representation is an exact technique but requires a doubling of the phase space that often leads to instabilities [27]. The TW is an approximate technique that typically has significantly longer convergence times than the positive-P representation. However, it makes an uncontrolled approximation [28] and, therefore, may converge to incorrect solutions. Both of these methods, along with all other coherent-state-based representations, experience difficulties dealing with large number-conserving nonlinearities as the underlying Gaussian basis becomes inappropriate. Such large number-conserving nonlinearities typically are the dominant energies in confined cold-atomic systems by a couple of orders of magnitude. Recently, we introduced a stochastic method based on a number-phase Wigner (NPW) representation [29], which provides a nonapproximate method for simulating large

number-conserving nonlinearities with dramatically improved convergence.

Modeling highly nonlinear systems undergoing continuous monitoring and feedback requires the simulation of a *conditional* quantum state. Continuous measurement of a quantum system can have a dramatic effect on its dynamics. In fact, the choice of measurement can even be used as a controlling mechanism by itself [30,31]. Therefore, it is unsurprising that the appropriate choice of phase-space representation is heavily influenced by the choice of measurement as it may drive the conditioned system toward a state that is simpler to describe in a particular representation. In a recent paper, we demonstrated how to unravel a particular form of stochastic Fokker-Planck equation (SFPE), which allows stochastic simulation techniques to apply to a class of conditional quantum systems [32]. It is only possible to generate SFPEs of this form with particular combinations of measurement schemes and phase-space representations. In particular, methods based on coherent-state representations are badly suited to measurements involving numberlike observables, which are prevalent in atom optics. In this paper, we show that the NPW representation produces dramatically superior results than coherent-state-based representations for these calculations.

A common quantum-atom-optical system under monitoring is governed by the conditional master equation,

$$d\hat{\rho} = -i[H(\boldsymbol{u}),\hat{\rho}]dt + \sum_i \mathcal{D}[\hat{L}_i]\hat{\rho}\,dt + \sum_i \mathcal{H}[\hat{L}_i]\hat{\rho}\,dW_i, \tag{1}$$

where $\mathcal{D}[\hat{c}]\hat{\rho} = \hat{c}\hat{\rho}\hat{c}^\dagger - \frac{1}{2}(\hat{c}^\dagger\hat{c}\hat{\rho} + \rho\hat{c}^\dagger\hat{c})$, dW is an Ito-Wiener increment, $\mathcal{H}[\hat{c}]\hat{\rho} = \hat{c}\hat{\rho} + \rho\hat{c}^\dagger - \langle\hat{c} + \hat{c}^\dagger\rangle\hat{\rho}$, $\langle\hat{c}\rangle = \mathrm{Tr}[\hat{c}\hat{\rho}]$ is our notation for a quantum expectation, $\hat{H}$ is the Hamiltonian and contains the contributions from kinetic energy, potential energy, many-body interactions and the controls, which are dependent on the set of feedback signals $\boldsymbol{u}$, and $\hat{L}_i = \int d\boldsymbol{x}\,\hat{\psi}^\dagger(\boldsymbol{x})L_i(\boldsymbol{x})\hat{\psi}(\boldsymbol{x})$ is the measurement operator where the functions $L_i(\boldsymbol{x})$ define measured density modes of the multimode field. We have restricted the measurement operators $\hat{L}_i$ such that they are algebraically numberlike in terms of the field operators. This form is the lowest-order number-conserving interaction possible for a multimode system. Measurements that are lower order with respect to the field operators do not conserve the number and may be suited to traditional coherent-state representations, but in many cases, these systems may be treated using analytic techniques, such as the Kalman filter, making simulation less important. Number-conserving measurements are quite common in engineered monitoring of BECs [14,15,33–38]. Typically, off-resonant light is used to image the density moments of a BEC. Dynamically gaining information from a BEC using this method is likely to be common as a further phase-sensitive measurement requires the existence of an atomic local oscillator to use as a phase standard, which is technically challenging. Thus, the efficient simulation of Eq. (1) will be relevant for a wide variety of atom-optical systems in the present and in the future.

In Sec. II, we apply the NPW method to a single-mode atom-optical system under a continuous number measurement, showing that it converges correctly over a long time scale. In Sec. III, we apply it to a two-mode Bose-Hubbard model, describing how the kinetic-energy terms can be approximated in the NPW method. In Sec. IV, we combine these two techniques to demonstrate the simulation of a multimode conditional atom-optical system, which has only been possible in the past by performing a semiclassical approximation [15].

II. CONDITIONAL EVOLUTION FOR A SINGLE-MODE SYSTEM

To analyze the simulation of Eq. (1) using NPW-based methods, we require a verifiable solution for comparison. As the measurement operator $\hat{L}_i$ is second order with respect to the field operators, Gaussian analytic techniques, such as the Kalman filter are not guaranteed to be exact [16], and we are forced to integrate the master equation directly to generate a benchmark for comparison. This restricts us to look at single-mode systems as direct integration is not scalable to multimode systems. A simple single-mode problem that is of the form of Eq. (1) is

$$d\hat{\rho} = \gamma\mathcal{D}[\hat{a}^\dagger\hat{a}]\hat{\rho}\,dt + \gamma\mathcal{C}[\hat{a}^\dagger\hat{a}]\hat{\rho}\,dt + \sqrt{\gamma}\mathcal{H}[\hat{a}^\dagger\hat{a}]\hat{\rho}\circ dW, \tag{2}$$

where $\circ dW$ is a Stratonovich-Wiener increment and we define the Stratonovich correction superoperator as $\mathcal{C}[\hat{c}]\hat{\rho} = \langle\hat{c} + \hat{c}^\dagger\rangle\mathcal{H}[\hat{c}]\hat{\rho} - \frac{1}{2}\mathcal{H}[\hat{c}^2]\hat{\rho} + \langle\hat{c}^\dagger\hat{c}\rangle\hat{\rho} - \hat{c}\hat{\rho}\hat{c}^\dagger$. This master equation describes a system undergoing continuous monitoring under a number measurement.

The scalability of stochastic techniques for solving conditional quantum dynamics has already been demonstrated in Ref. [32], but we aim to investigate the effect of choosing different representations. We use master equation (2) to compare the performance of leading coherent-based scalable stochastic methods to the NPW representation. The convergence of these techniques is compared to a direct integration of the master equation.

Coherent-state-based representations, positive-P and TW have been successful at describing the evolution of BEC and quantum-optical systems. Starting with the positive-P representation, we now investigate the applicability of these techniques on a *conditional* master equation. Using the correspondences in Ref. [19], we can convert master equation (2) to

$$\begin{aligned} d\mathcal{P}(\boldsymbol{\alpha}) = \{&\gamma[\partial_\alpha\alpha(1 + 2|\alpha|^2 - 2\mathbb{E}_\mathcal{P}[|\alpha|^2]) - \partial_\alpha^2\alpha^2 \\ &+ \partial_{\alpha^*}\alpha^*(1 + 2|\alpha|^2 - 2\mathbb{E}_\mathcal{P}[|\alpha|^2]) - \partial_{\alpha^*}^2(\alpha^*)^2 \\ &- 2(|\alpha|^2 + |\alpha|^4 - \mathbb{E}_\mathcal{P}[|\alpha|^2] - \mathbb{E}_\mathcal{P}[|\alpha|^4]) \\ &+ 4\mathbb{E}_\mathcal{P}[|\alpha|^2](|\alpha|^2 - \mathbb{E}_\mathcal{P}[|\alpha|^2])]dt \\ &+ \sqrt{\gamma}[-\partial_\alpha\alpha - \partial_{\alpha^*}\alpha^* \\ &+ 2(|\alpha|^2 - \mathbb{E}_\mathcal{P}[|\alpha|^2])] \circ dW\}\mathcal{P}(\boldsymbol{\alpha}), \end{aligned} \tag{3}$$

where $\mathcal{P}(\boldsymbol{\alpha})$ is the P-representation quasiprobability distribution that reproduces normally ordered moments of master equation (2) and $\mathbb{E}_\mathcal{Q}[f(\boldsymbol{x})] \equiv \int d\boldsymbol{x}\,f(\boldsymbol{x})\mathcal{Q}(\boldsymbol{x})$ is our notation for taking the expectation values of a function $f(\boldsymbol{x})$ with respect to the quasiprobability distribution $\mathcal{Q}(\boldsymbol{x})$. We note that this equation contains nonpositive definite diffusion that must be simulated by doubling the phase space. Thus, positive-P techniques are required. This representation can

then be unravelled into the following set of stochastic equations [32]:

$$\begin{aligned} d\alpha_p &= -2\gamma\alpha_p(\alpha_p^+\alpha_p - \mathbb{E}_f[\alpha_p^+\alpha_p])dt \\ &\quad + \sqrt{\gamma}\alpha_P \circ (i\,dV_1 + i\,dV_2 + dW), \\ d\alpha_p^+ &= -2\gamma\alpha_p^+(\alpha_p^+\alpha_p - \mathbb{E}_f[\alpha_p^+\alpha_p])dt \\ &\quad + \sqrt{\gamma}\alpha_p^+ \circ (-i\,dV_1 + i\,dV_2 + dW), \\ d\omega_p &= -2\gamma\omega_p\{\alpha_p^+\alpha_p + (\alpha_p^+)^2\alpha_p^2 - 2\alpha_p^+\alpha_p\mathbb{E}_f[\alpha_p^+\alpha_p]\}dt \\ &\quad + 2\sqrt{\gamma}\omega_p\alpha_p^+\alpha_p \circ dW, \end{aligned} \tag{4}$$

where dV_1 and dV_2 are a set of fictitious noises that are averaged over to obtain the weighted averages $\mathbb{E}_f[f(\boldsymbol{x})] \equiv \sum_i \omega_i f(\boldsymbol{x}_i)/\sum_i \omega_i$ [32]. Equations (4) will be used to benchmark the unravelling of Eq. (2) using coherent-state-based methods.

Now, consider the TW representation. Using the operator correspondences given in Ref. [19], we can write the master equation for the Wigner quasiprobability distribution $\mathcal{W}(\boldsymbol{\alpha})$ as

$$\begin{aligned} d\mathcal{W}(\boldsymbol{\alpha}) = \big[&\gamma\big(-\tfrac{1}{2}\partial_\alpha^2\alpha^2 - \tfrac{1}{2}\partial_{\alpha^*}^2(\alpha^*)^2 + \partial_{\alpha^*}\partial_\alpha|\alpha|^2 \\ &+ (\partial_{\alpha^*}\partial_\alpha + 4\mathbb{E}_{\mathcal{W}}[|\alpha|^2])(|\alpha|^2 - \mathbb{E}_{\mathcal{W}}[|\alpha|^2]) \\ &- 2(|\alpha|^4 - \mathbb{E}_{\mathcal{W}}[|\alpha|^4]) - \tfrac{1}{8}\partial_{\alpha^*}^2\partial_\alpha^2\big)dt \\ &+ \big(-\tfrac{1}{2}\partial_{\alpha^*}\partial_\alpha + 2(|\alpha|^2 - \mathbb{E}_{\mathcal{W}}[|\alpha|^2])\big) \circ dW\big] \\ &\times \mathcal{W}(\boldsymbol{\alpha}). \end{aligned} \tag{5}$$

Note that the first term contains higher-order derivatives, and a truncation is required in order to obtain a stochastic unravelling of Eq. (5). Note also that a positive-P-representation-style extension of the phase space would be required to simulate the diffusion in the conditioning term. Traditionally, the Wigner representation is guaranteed to produce strictly positive-definite diffusion [19], but this is under the assumption that the calculus increment is positive as is the case with dt. Unfortunately, this assumption does not hold with the dW increment. A new positive Wigner representation could be derived by analogy to the positive-P representation, but the higher-order terms would still need to be truncated. This would make this hypothetical representation both approximate *and* doubled in phase space, which would make it unlikely to compete with the positive-P representation. Thus, it is not worthy of further investigation.

Finally, we consider the NPW representation. The NPW was first derived in Ref. [29] and was used in the simulation of large nonlinear quantum systems. We now consider its applicability for use on *conditioned* atom-optical systems. Using the operator correspondences given in Ref. [29], we get the following equation:

$$\begin{aligned} d\mathcal{N}(n,\phi) = \big[&\gamma\big(\tfrac{1}{2}\partial_\phi^2 - 2(n^2 - \mathbb{E}_{\mathcal{N}}[n^2]) \\ &+ 4\mathbb{E}_{\mathcal{N}}[n](n - \mathbb{E}_{\mathcal{N}}[n]))dt \\ &+ 2\sqrt{\gamma}\big(n - \mathbb{E}_{\mathcal{N}}[n]\big) \circ dW\big]\mathcal{N}(n,\phi), \end{aligned} \tag{6}$$

where $\mathcal{N}(n,\phi)$ is the NPW representation that produces a complete set of moments of the master equation as outlined in Ref. [29]. We next unravel Eq. (6) using Ref. [32] to

$$\begin{aligned} &dn = 0, \quad d\phi = \sqrt{\gamma} \circ dV_1, \\ &d\omega_n = \gamma\omega(-2n^2 + 4\mathbb{E}_f[n]n)dt + 2\sqrt{\gamma}\omega n \circ dW. \end{aligned} \tag{7}$$

Note we did not need to apply any truncations or double the phase space. The simplicity of Eqs. (7) compared to Eq. (4) show how an appropriate choice of representation, the NPW in this case, can greatly reduce the complexity of the evolution, just as an appropriate choice of basis can simplify analysis of other quantum problems.

We emphasize the simplicity of Eq. (6) compared to Eq. (5) is not simply due to a coordinate transformation, but rather, it originates from a fundamental difference in the construction of the representations. Evolution of transformed quasidistributions has been considered in the Q representation [34], and for the tomographic Wigner distribution [39], however, these approaches would not help in this situation as they cannot fix the non-semi-positive-definite diffusion in Eq. (5).

We can now compare the performances of the NPW and the positive-P representations by integrating Eqs. (4) and (7), respectively. The results of these simulations, together with a direct integration of the master equation, are shown in Fig. 1. The NPW representation converges until a complete collapse into the correct number state. As this is the steady state of the equation, we expect the NP representation to converge indefinitely [see Fig. 1(a)]. The NPW also produces significantly smaller errors and uncertainty as compared to the positive-P representation [Figs. 1(a,ii) and 1(b,ii)]. The decrease in the uncertainty reduces the error of the evolution as the simulation of the conditional master equation uses an estimate of the observable $\langle\hat{c} + \hat{c}^\dagger\rangle$, thus, the increased uncertainty in the results increases the error in the long term. This dynamic instability is not seen in unconditioned master equation evolution and makes the uncertainty of stochastic techniques considerably more important in these problems.

We have demonstrated the accuracy and advantage of the NPW representation for conditional simulations using the single-mode model, Eq. (2), as a benchmark. However, to simulate realistic BEC models, we also would need to include both the kinetic-energy and the nonlinear interaction terms in the Hamiltonian. Just like the measurement considered in this section, the nonlinear term has a numberlike form, which, therefore, is well suited to being solved using the NPW representation. However, the kinetic-energy term, which is normally trivial for coherent-state-based representations, requires approximations to be solved via the NPW method. In the next section, we examine these approximations in the context of the simplest multimode model with both coupling and nonlinear terms.

III. TWO-MODE BOSE-HUBBARD MODEL

We describe how to deal with coupling terms within the NPW method by examining the simplest nontrivial model. We consider two coupled anharmonic oscillators corresponding to

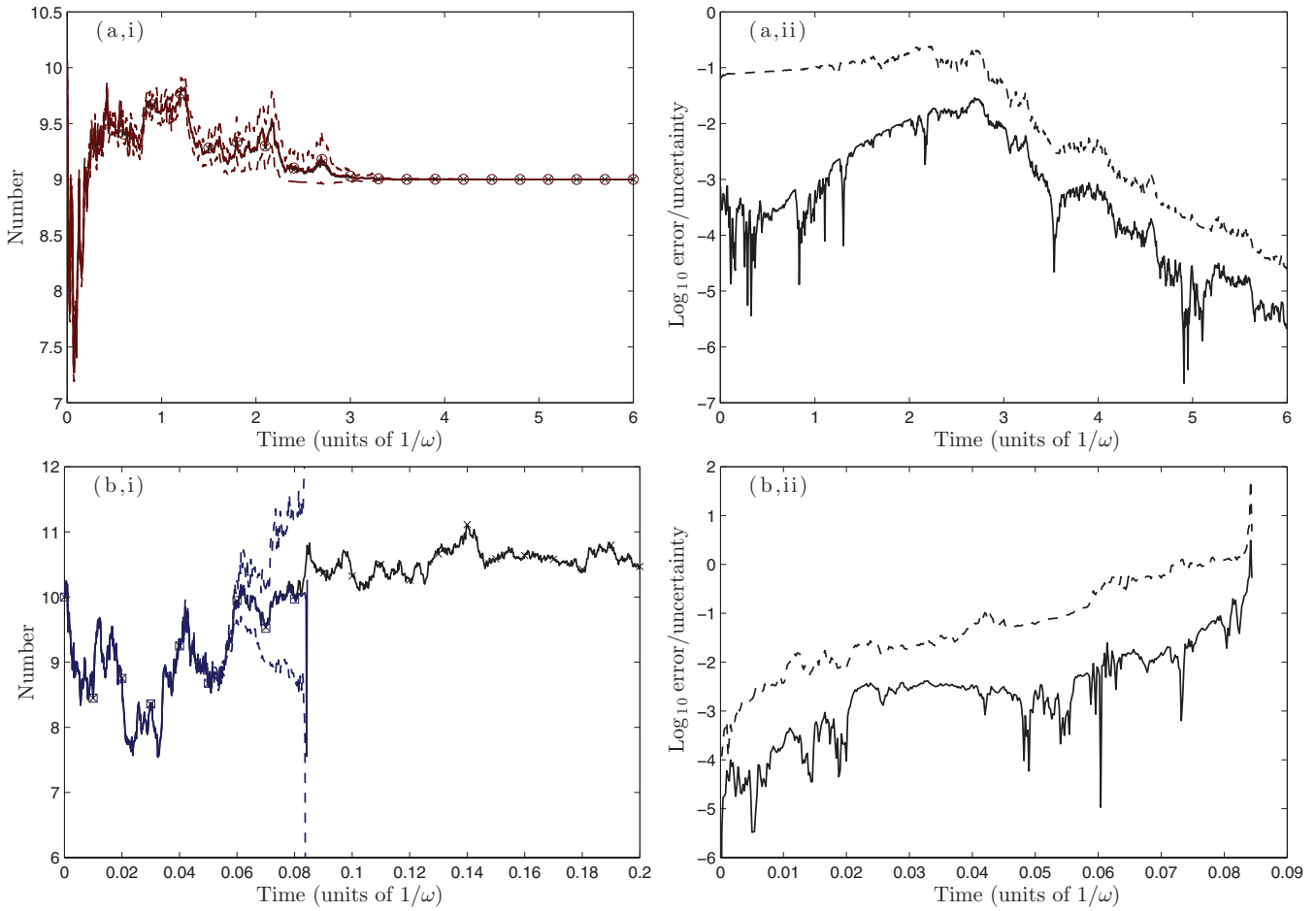

FIG. 1. (Color online) Average number of quanta as a function of time for the stochastic simulations using the NPW [red circles in (a,i)] and the positive-P representation [blue squares in (b,i)] for an initial coherent state with amplitude 10, both have a 2σ confidence interval plotted with dashed lines. The results for the direct integration of the master equation (7) are shown in both plots for comparison (black crosses). The positive-P representation results diverge after $t \approx 0.15/\omega$ and are not plotted beyond this point. Plots (a,ii) and (b,ii) show, on a logarithmic scale, the errors (solid black lines) defined as the difference between each stochastic result and the exact solution and the uncertainty (dashed black line) defined as the standard deviation in the averages, corresponding to plots (a,i) and (b,i), respectively. The NPW simulation is considerably more precise and is convergent for at least an order of magnitude longer than the positive-P representation.

the Hamiltonian of the Bose-Hubbard model truncated to two sites,

$$\hat{H} = \kappa(\hat{a}^\dagger \hat{b} + \hat{b}^\dagger \hat{a}) + \frac{\chi}{2}[(\hat{a}^\dagger \hat{a})^2 + (\hat{b}^\dagger \hat{b})^2], \tag{8}$$

where $\hat{a}$ and $\hat{b}$ are the annihilation operators for the two modes. The first term represents the coupling between the two sites, whereas, the second one contains the nonlinearity. This Hamiltonian describes the dynamics of a condensate in a double-well potential and has been studied thoroughly with a variety of methods both experimentally [40,41] and theoretically [42–44]. Although, in general, the system is not solvable analytically, it can be integrated directly, and we use this solution as a benchmark for comparison between coherent-state- and NP-based methods.

The various phase-space representations will deal differently with the nonlinear and coupling terms of the Hamiltonian (8). The NPW treats the nonlinearity *exactly*, whereas, the coherent methods treat the coupling term in an exact way. The methods by which the positive-P representation and the TW simulate the nonlinear term are known: The positive-P representation requires a doubling of the phase space, and the TW requires a truncation of higher-order differential terms. We now present the analysis of the approximations needed to simulate the kinetic term with the NPW representation.

A. The kinetic term in the NPW representation

We start our investigation by considering the equation of motion for the NPW representation [29] generated from the Hamiltonian in Eq. (8),

$$\partial_t \mathcal{N}(\boldsymbol{n},\boldsymbol{\phi}) = \kappa \left(\sqrt{n_a + \frac{i}{2}\partial_{\phi_a}}\, e^{-i\phi_a} \sqrt{n_b + 1 + \frac{i}{2}\partial_{\phi_b}}\, e^{i\phi_b} \right.$$
$$\times \left\{ \mathcal{N}\left(n_a - \frac{1}{2}, n_b + \frac{1}{2}, \phi_a, \phi_b\right) \right.$$
$$\left. \left. - \int_0^{2\pi} d\phi_b' \exp\left[2i(\phi_b - \phi_b')\left(n_b + \frac{1}{2}\right)\right] \right.\right.$$

$$\times \mathcal{N}\left(n_a-\frac{1}{2},n_b+\frac{1}{2},\phi_a,\phi_b'\right)\Big\}$$
$$\times\sqrt{n_b+\frac{i}{2}\partial_{\phi_b}}e^{-i\phi_b}\sqrt{n_a+1+\frac{i}{2}\partial_{\phi_a}}e^{i\phi_a}$$
$$\times\Big\{\mathcal{N}\left(n_a+\frac{1}{2},n_b-\frac{1}{2},\phi_a,\phi_b\right)$$
$$-\int_0^{2\pi}d\phi_a'\exp\left[2i(\phi_a-\phi_a')\left(n_a+\frac{1}{2}\right)\right]$$
$$\times\mathcal{N}\left(n_a+\frac{1}{2},n_b-\frac{1}{2},\phi_a',\phi_b\right)\Big\}\Big)$$
$$+\chi\left(\partial_{\phi_a}n_a+\partial_{\phi_b}n_b\right)\mathcal{N}(\boldsymbol{n},\boldsymbol{\phi}). \quad (9)$$

As it stands, this equation is not of a Fokker-Planck type; it is not classically Markovian and cannot be unravelled into a set of stochastic differential equations (SDEs). To fix this situation, we apply a set of approximations that sets the evolution in the form of an FPE, which can then be unravelled into SDEs in a scalable manner.

First note that the integral terms can be seen as the overlap between the state and the vacuum,

$$\int_0^{2\pi}d\phi'\exp\left[-2i\phi'\left(n+\frac{1}{2}\right)\right]\mathcal{N}\left(n+\frac{1}{2},\phi'\right)$$
$$=\langle 0|\hat{\rho}|2n+1\rangle. \quad (10)$$

Now, assume that the states generated by the dynamics are highly exited states, such as large coherent or number states. These states have little overlap with the vacuum, and we, thus, can neglect the integrals. This approximation is valid for states with large n and can be thought of as approaching the semiclassical limit. This is akin to the truncation performed in the coherent Wigner representation, which also is valid in the large n limit. The evolution then reduces to

$$\partial_t\mathcal{N}(\boldsymbol{n},\boldsymbol{\phi})=\kappa\left(\sqrt{n_a+\frac{i}{2}\partial_{\phi_a}}e^{-i\phi_a}\sqrt{n_b+1+\frac{i}{2}\partial_{\phi_b}}e^{i\phi_b}\right)$$
$$\times\mathcal{N}\left(n_a-\frac{1}{2},n_b+\frac{1}{2},\phi_a,\phi_b\right)$$
$$\times\left(\sqrt{n_b+\frac{i}{2}\partial_{\phi_b}}e^{-i\phi_b}\sqrt{n_a+1+\frac{i}{2}\partial_{\phi_a}}e^{i\phi_a}\right)$$
$$\times\mathcal{N}\left(n_a+\frac{1}{2},n_b-\frac{1}{2},\phi_a,\phi_b\right)$$
$$+\chi\left(\partial_{\phi_a}n_a+\partial_{\phi_b}n_b\right)\mathcal{N}(\boldsymbol{n},\boldsymbol{\phi}). \quad (11)$$

Next, we must expand the square roots present in Eq. (11) using a Taylor-series expansion. For example,

$$\sqrt{n+\frac{i}{2}\partial_\phi}\approx\sqrt{n}+i\frac{1}{4\sqrt{n}}\partial_\phi+\frac{1}{32\sqrt{n^3}}\partial_\phi^2+\cdots. \quad (12)$$

Expanding the square roots will generate terms with different orders of partial derivatives with respect to ϕ. Since we are assuming that n is large, we also neglect all the terms with prefactors of order at least $1/n^2$. Now, we can group the terms of the same order and can analyze them individually. First, we consider the zeroth-order term,

$$\partial_t\mathcal{N}(\boldsymbol{n},\boldsymbol{\phi})=2\kappa\,\sin(\phi_b-\phi_a)$$
$$\times\left[\sqrt{n_a(n_b+1)}\mathcal{N}\left(n_a-\frac{1}{2},n_b+\frac{1}{2},\phi_a,\phi_b\right)\right.$$
$$\left.-\sqrt{n_b(n_a+1)}\mathcal{N}\left(n_a+\frac{1}{2},n_b-\frac{1}{2},\phi_a,\phi_b\right)\right]$$
$$+\cdots. \quad (13)$$

As the number variable is quantized, we would anticipate the evolution of this variable to involve jumps of some kind. However, interpreting the expression above in terms of jump processes would necessarily lead to jumps occurring with negative probabilities. To avoid this problem, we take n to the continuum limit [45] and set $\mathcal{N}(n_a\pm\frac{1}{2},n_b\mp\frac{1}{2},\phi_a,\phi_b)\approx\mathcal{N}(\boldsymbol{n},\boldsymbol{\phi})$. Using this and the finite-difference approximation,

$$f\left(x+\frac{1}{2}h\right)-f\left(x-\frac{1}{2}h\right)=hf'(x)+O(h^3), \quad (14)$$

we find that the zeroth-order term simplifies to

$$\partial_t\mathcal{N}(\boldsymbol{n},\boldsymbol{\phi})\approx 2\kappa\left(\partial_{n_b}-\partial_{n_a}\right)\sin(\phi_b-\phi_a)$$
$$\times\sqrt{\left(n_a+\tfrac{1}{2}\right)\left(n_b+\tfrac{1}{2}\right)}\mathcal{N}(\boldsymbol{n},\boldsymbol{\phi})+\cdots. \quad (15)$$

For the first-order terms,

$$\partial_t\mathcal{N}(\boldsymbol{n},\boldsymbol{\phi})=\cdots+2\kappa\,\partial_{\phi_a}\cos(\phi_b-\phi_a)$$
$$\times\left[\frac{\sqrt{n_b+1}}{4\sqrt{n_a}}\mathcal{N}\left(n_a-\frac{1}{2},n_b+\frac{1}{2},\phi_a,\phi_b\right)\right.$$
$$\left.+\frac{\sqrt{n_b}}{4\sqrt{n_a+1}}\mathcal{N}\left(n_a+\frac{1}{2},n_b-\frac{1}{2},\phi_a,\phi_b\right)\right]$$
$$+2\kappa\,\partial_{\phi_b}\cos(\phi_b-\phi_a)$$
$$\times\left[\frac{\sqrt{n_a+1}}{4\sqrt{n_b}}\mathcal{N}\left(n_a+\frac{1}{2},n_b-\frac{1}{2},\phi_a,\phi_b\right)\right.$$
$$\left.+\frac{\sqrt{n_a}}{4\sqrt{n_b+1}}\mathcal{N}\left(n_a-\frac{1}{2},n_b+\frac{1}{2},\phi_a,\phi_b\right)\right]$$
$$+\cdots, \quad (16)$$

we will also take the continuum n limit. Note that we do not have to use the finite-difference approximation since only finite sums appear in this term. The result is

$$\partial_t\mathcal{N}(\boldsymbol{n},\boldsymbol{\phi})\approx\cdots+\kappa\left(\partial_{\phi_a}\frac{\sqrt{n_b+\frac{1}{2}}}{\sqrt{n_a+\frac{1}{2}}}+\partial_{\phi_b}\frac{\sqrt{n_a+\frac{1}{2}}}{\sqrt{n_b+\frac{1}{2}}}\right)$$
$$\times\cos(\phi_b-\phi_a)\mathcal{N}(\boldsymbol{n},\boldsymbol{\phi})+\cdots. \quad (17)$$

Finally, the same continuum approximation cancels out all the diffusion terms in the second-order term. These approximations give us the following Markovian evolution for our NPW representation:

$$\partial_t\mathcal{N}(\boldsymbol{n},\boldsymbol{\phi})=\left\{\kappa\left[2\left(\partial_{n_b}-\partial_{n_a}\right)\sqrt{\left(n_a+\frac{1}{2}\right)\left(n_b+\frac{1}{2}\right)}\right.\right.$$
$$\times\sin(\phi_b-\phi_a)$$

$$+\left(\partial_{\phi_a}\frac{\sqrt{n_b+\frac{1}{2}}}{\sqrt{n_a+\frac{1}{2}}}+\partial_{\phi_b}\frac{\sqrt{n_a+\frac{1}{2}}}{\sqrt{n_b+\frac{1}{2}}}\right)\times\cos(\phi_b-\phi_a)\Bigg]+\chi\left(\partial_{\phi_a}n_a+\partial_{\phi_b}n_b\right)\Bigg\}\mathcal{N}(\boldsymbol{n},\boldsymbol{\phi}). \tag{18}$$

Equation (18) is in Fokker-Planck form and can now be unravelled into the following set of SDEs for scalable simulation:

$$\begin{aligned}
dn_a &= 2\kappa\,\sin(\phi_b-\phi_a)\sqrt{\left(n_a+\frac{1}{2}\right)\left(n_b+\frac{1}{2}\right)}dt,\\
dn_b &= -2\kappa\,\sin(\phi_b-\phi_a)\sqrt{\left(n_a+\frac{1}{2}\right)\left(n_b+\frac{1}{2}\right)}dt,\\
d\phi_a &= \left(-\cos(\phi_b-\phi_a)\frac{\sqrt{n_b+\frac{1}{2}}}{\sqrt{n_a+\frac{1}{2}}}+\chi n_a\right)dt,\\
d\phi_b &= \left(-\cos(\phi_b-\phi_a)\frac{\sqrt{n_a+\frac{1}{2}}}{\sqrt{n_b+\frac{1}{2}}}+\chi n_b\right)dt.
\end{aligned} \tag{19}$$

If we consider the transformation where we set $\alpha_n=\sqrt{n_a+\frac{1}{2}}e^{i\phi_a}$ and $\beta_n=\sqrt{n_b+\frac{1}{2}}e^{i\phi_b}$, which corresponds to the operator expectations $\langle\hat{a}\rangle$ and $\langle\hat{b}\rangle$, respectively, we get the following set of equations:

$$\begin{aligned}
d\alpha_n &= -i\left[\kappa\beta_n+\chi\left(|\alpha_n|^2-\tfrac{1}{2}\right)\alpha_n\right]dt,\\
d\beta_n &= -i\left[\kappa\alpha_n+\chi\left(|\beta_n|^2-\tfrac{1}{2}\right)\beta_n\right]dt.
\end{aligned} \tag{20}$$

Note that, as mentioned before, in the limit where there is no coupling ($\kappa=0$), the equations are exact. What is curious here is that, in the opposite limit, i.e., when there is no nonlinearity and only coupling ($\chi=0$), Eqs. (20) perfectly match the mean-field evolution and are exact. Therefore, Eqs. (20) are correct in both extreme limits.

Note also that Eqs. (20) are equivalent to the equations of motion for the mean-field evolution of Eq. (8) up to an absolute phase rotation. Thus, in a similar sense to the TW representation, by taking the large n limit, we have entered the semiclassical regime. We find that the difference in evolution between TW, mean field, and NPW is entirely due to the effects of the random sampling of the initial condition.

B. Initial sampling

In a previous paper, we showed that number states can be sampled in a scalable and exact way [29] as a number state $|n_0\rangle$ is given by the strictly positive distribution,

$$\mathcal{N}_{n_0}(n,\phi)=\frac{1}{2\pi}\delta_{n,n_0}. \tag{21}$$

Coherent states, on the other hand, have distributions that are not strictly positive [29]. Fortunately, this can be fixed in the large n limit as shown in Appendix A. A coherent state $|\alpha_0\rangle$, where $\alpha_0=r_0e^{i\phi_0}$, is given by

$$\mathcal{N}_{\alpha_0}(n,\phi)=\frac{r_0^n\exp\left[-n_0+\frac{-2(\phi-\phi_0)^2}{\psi^{(1)}(n+1)}\right]\sqrt{2}}{n!\sqrt{\pi\psi^{(1)}(n+1)}}, \tag{22}$$

where $\psi^{(1)}(n+1)$ is the trigamma function and n is an integer $n=0,1,2,\ldots$, as we have eliminated the half-integer contribution as a weaker approximation on the way toward the continuum limit. This expression allows us to sample coherent states in a scalable and efficient way as it is strictly positive, and it is the product of a Poissonian and Gaussian distribution. Combining these sampling techniques and the dynamic equations (19), we can simulate the Hamiltonian (8).

C. Evolution and sampling of the TW method

For the TW, the dynamical equation obtained from standard techniques [18,19] is given by

$$\begin{aligned}
\partial_t\mathcal{W}(\boldsymbol{\alpha},\boldsymbol{\beta}) = \Bigg[&i\partial_\alpha\left(\frac{\chi}{2}(2|\alpha|^2-1)\alpha+\kappa\beta\right)\\
&-i\partial_{\alpha^*}\left(\frac{\chi}{2}(2|\alpha|^2-1)\alpha^*+\kappa\beta^*\right)\\
&+i\partial_\beta\left(\frac{\chi}{2}(2|\beta|^2-1)\beta+\kappa\alpha\right)\\
&-i\partial_{\beta^*}\left(\frac{\chi}{2}(2|\beta|^2-1)\beta^*+\kappa\alpha^*\right)\\
&-i\frac{\chi}{4}\left(\partial_{\alpha^*}\partial_\alpha\partial_\alpha\alpha-\partial_{\alpha^*}\partial_{\alpha^*}\partial_\alpha\alpha^*\right)\\
&-i\frac{\chi}{4}(\partial_{\beta^*}\partial_\beta\partial_\beta\beta-\partial_{\beta^*}\partial_{\beta^*}\partial_\beta\beta^*)\Bigg]\\
&\times\mathcal{W}(\boldsymbol{\alpha},\boldsymbol{\beta}),
\end{aligned} \tag{23}$$

and generates the following SDEs:

$$\begin{aligned}
d\alpha_w &= -i\left(\frac{\chi}{2}(2|\alpha_w|^2-1)\alpha_w+\kappa\beta_w\right)dt,\\
d\beta_w &= -i\left(\frac{\chi}{2}(2|\beta_w|^2-1)\beta_w+\kappa\alpha_w\right)dt.
\end{aligned} \tag{24}$$

As noted before, the equations are the same as the mean field and the NPW representation as shown in Eq. (20), and the difference lies in the initial sampling. For the TW representation, coherent states $|\alpha_0\rangle$ are straightforward to sample, and we sample them using the distribution [18],

$$\mathcal{W}_{\alpha_0}(\boldsymbol{\alpha})=\frac{2}{\pi}e^{-|\alpha-\alpha_0|^2}. \tag{25}$$

On the other hand, when a number state is treated exactly, there is negativity in the distribution and cannot be sampled efficiently. Number states, however, can be treated in an approximate way using the result from [46,47]

$$\mathcal{W}_{n_0}=\sqrt{\frac{2}{\pi}}\exp\left[-2\left(|\alpha|^2-n_0-\frac{1}{2}\right)^2\right]. \tag{26}$$

With this, we can sample, then we can simulate, the Hamiltonian (8) using the TW representation.

D. Evolution and sampling of the positive-P representation method

For the positive-P representation, the evolution is [18,19]

$$\begin{aligned}\partial_t \mathcal{P}(\boldsymbol{\alpha},\boldsymbol{\beta}) = i\Big[&\partial_\alpha\Big(\kappa\beta - \frac{\chi}{2}(1+2|\alpha|^2)\alpha\Big)\\ &- \partial_{\alpha^*}\Big(\kappa\beta^* - \frac{\chi}{2}(1+2|\alpha|^2)\alpha^*\Big)\\ &+ \partial_\beta\Big(\kappa\alpha - \frac{\chi}{2}(1+2|\beta|^2)\beta\Big)\\ &- \partial_{\beta^*}\Big(\kappa\alpha^* - \frac{\chi}{2}(1+2|\beta|^2)\beta^*\Big)\\ &+ \partial_\alpha^2\alpha^2 - \partial_{\alpha^*}^2(\alpha^*)^2 + \partial_\beta^2\beta^2 - \partial_{\beta^*}(\beta^*)^2\Big]\\ &\times \mathcal{P}(\boldsymbol{\alpha},\boldsymbol{\beta}). \end{aligned} \tag{27}$$

The diffusion terms are not positive semidefinite, thus, we must double the phase space to get the following SDEs:

$$\begin{aligned} d\alpha_p &= -i\left(\kappa\beta_p + \chi\alpha_p^2\alpha_p^+\right)dt + \sqrt{-i\chi}\circ dW_1,\\ d\alpha_p^+ &= i[\kappa\beta_p^+ + \chi\alpha_p(\alpha_p^+)^2]dt + \sqrt{i\chi}\circ dW_2,\\ d\beta_p &= -i\left(\kappa\alpha_p + \chi\beta_p^2\beta_p^+\right)dt + \sqrt{-i\chi}\circ dW_3,\\ d\beta_p^+ &= i[\alpha_p^+ + \chi\beta_p(\beta_p^+)^2]dt + \sqrt{i\chi}\circ dW_4, \end{aligned} \tag{28}$$

where α_p^+ and β_p^+ are the doubled variables for the positive-P representation. We note that α_p^+ and β_p^+ initially are set to be complex conjugates of α_p^+ and β_p^+, respectively, when sampling coherent states. Explicitly, the positive-P representation of a coherent state $|\alpha_0\rangle$ is,

$$\mathcal{P}_{\alpha_0}(\boldsymbol{\alpha},\boldsymbol{\alpha}^+) = \delta(\alpha_0 - \boldsymbol{\alpha})\delta(\alpha_0^* - \boldsymbol{\alpha}^+). \tag{29}$$

Much like the TW representation sampling, a number state requires special treatment. The P distribution of a number state is the derivative of a δ function, which cannot be sampled in a scalable way. Instead, we take advantage of the freedom provided by doubling the phase space and use a technique detailed in Refs. [46,48], which uses the distribution,

$$\mathcal{P}_{\alpha_0}(\boldsymbol{\alpha},\boldsymbol{\alpha}^+) = \frac{|\alpha - \alpha^+|^{2n}\exp\left(-\frac{|\alpha+\alpha^+|^2+|\alpha-\alpha^+|^2}{4}\right)}{4^n\pi^2 n!}. \tag{30}$$

We note that even the initial sampling of α_p^+ will not necessarily be the complex conjugate of α_p using Eq. (30). With these equations, we can simulate the Hamiltonian (8) using the positive-P representation.

E. Numerical comparison of stochastic methods

With the techniques described earlier in this section, we now are able to simulate the Bose-Hubbard Hamiltonian (8) and to compare the NPW, the TW, the positive-P representation, and the direct integration of the master equation. Since the NPW is exact for both the $\kappa = 0$ and the $\chi = 0$ regimes, we concentrate here on the intermediate regime where $\chi = \kappa$ to investigate the performance of the methods. Figure 2(a) shows the dynamics of an initial coherent state, whereas, Fig. 2(b) shows an initial number state. In both cases, the positive-P representation diverges early in the evolution due to instability

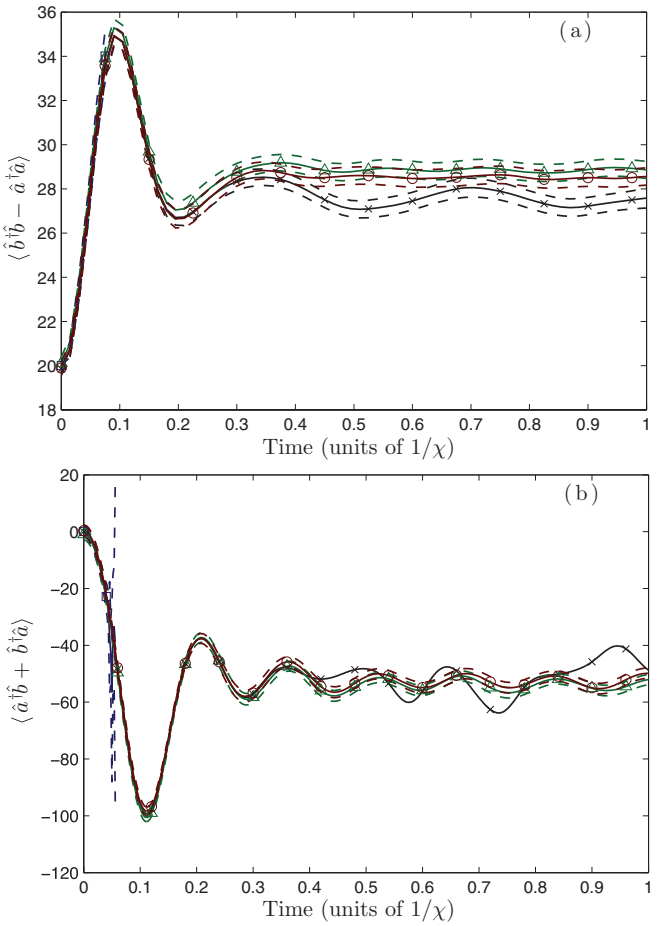

FIG. 2. (Color online) Comparison of the NPW (red, circles), the positive-P representation (blue, dashed lines), and the TW (green, triangles) methods for simulating the system given by the Hamiltonian (8). The result of a direct simulation of the master equation is shown in black with crosses. Plot (a) shows the evolution of the population difference for an initial coherent state with $\langle a^\dagger a\rangle = 90$ and $\langle b^\dagger b\rangle = 110$. Plot (b) shows the evolution of the observable $\langle a^\dagger b + b^\dagger a\rangle$ for an initial number state of 100 particles in each mode. In both cases, the positive-P representation solution diverges quickly, and the TW and the NPW methods have essentially identical convergence properties, following one or more oscillations before diverging from the exact evolution.

created by doubling the phase space, whereas, the NPW and the TW perform equally well, reproducing the correct behavior for some time. At this intermediate regime, it is not surprising that the NPW performs on par with the TW since the stochastic equations are the same with the methods differing only at the initial sampling stage.

However, it is interesting to see that this similarity between the NPW and the TW performances remains true for the whole range of χ/κ. Even in the Mott-insulator regime, where nonlinearity dominates and one would expect the NPW to perform better, both methods perform on par. As we move from $\kappa = 0$ to a finite value of κ, it seems that the number states cease to be the adequate basis of the problem, and the advantage of the NPW disappears. This is probably due to the strong approximations used to deal with the kinetic term that

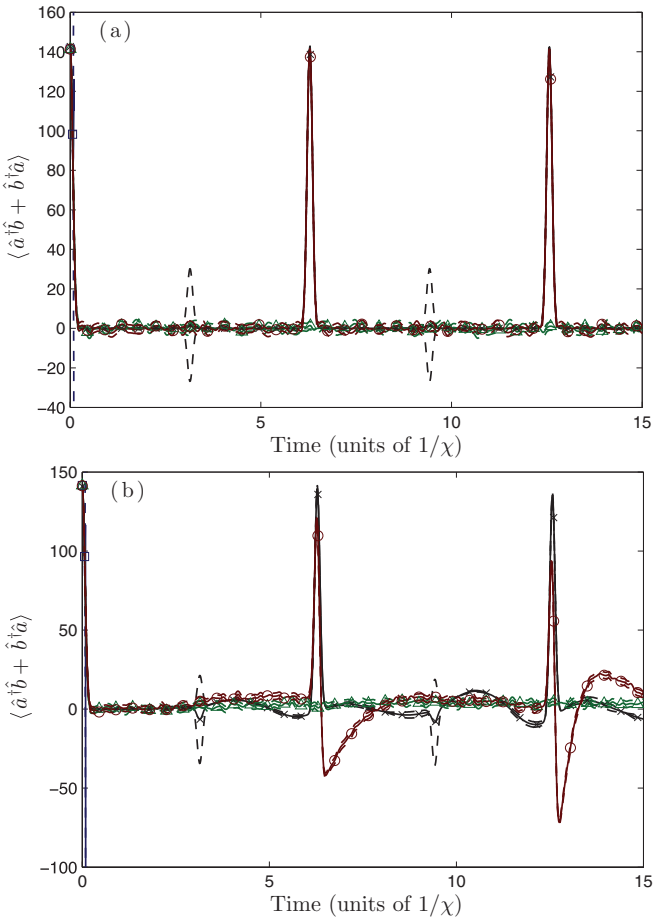

FIG. 3. (Color online) Investigation of the rephasing in the Bose-Hubbard model for an initial coherent state with $\langle a^\dagger a \rangle = \langle b^\dagger b \rangle = 100$. The NPW is plotted with (red) circles, the TW is plotted with (green) triangles, the positive-P representation is plotted with (blue) squares, and a direct integration of the master equation is plotted with (black) crosses. All plots have dashed lines indicating a 2σ confidence interval. In the absence of coupling [(a) with $\chi = 1$ and $\kappa = 0$], the NPW is exact and reproduces the revivals, whereas, the other methods completely miss them. When even a small coupling is introduced [(b) with $\chi/\kappa = 10^3$], the NPW loses its ability to reproduce the revivals in a quantitative manner.

set the NPW far into the semiclassical regime and close to the TW method.

This behavior is illustrated in Fig. 3 where we consider the rephasing of the Bose-Hubbard model. Even with the approximations applied to sample the initial coherent state, the NPW representation still successfully shows the rephasing in the absence of coupling ($\kappa = 0$). This is consistent with the result in Ref. [29] where we demonstrated that the NPW was superior to the TW and the positive-P representation to reproduce the revivals of a damped anharmonic oscillator. However, we see that the addition of even a very small coupling decreases the quality of the rephasing to a qualitative rather than a quantitative fit. The advantage of the NPW representation as a simulation tool for large coherent nonlinearities appears to be lost almost immediately.

The approximations used to restore Markovian dynamics to the NPW representation appear to be quite aggressive. This brings the NPW representation in line with the TW representation for Bose-Hubbard-style systems in terms of performance. However, as an additional advantage, the semiclassical nature of the approximation makes the NPW representation work significantly better in the superfluid regime than anticipated. In fact, as shown before, the NPW is exact only when coupling is present.

IV. MULTIMODE SYSTEM

In Sec. II, we demonstrated the accuracy and advantage of the NPW representation for conditional quantum systems, and in Sec. III, we devised a method of handling linear-coupling terms in multimode quantum systems. We saw that the NPW method produced simulations for the conditional system that were stable for orders of magnitude longer than any competing method but that convergence for the multimode Bose-Hubbard model was only a minor improvement over a carefully applied approximate TW method, except in extreme parameter limits. This difference is very straightforward to understand. For extremely large or small nonlinearities, the dynamics of the Bose-Hubbard model are simple and easily are expressed in terms of number and phase parameters (or indeed, coherent states for the low-nonlinearity limit). For intermediate parameter regimes, neither Gaussian nor NP states are an appropriate basis for the system, and the stochastic methods do not exhibit long-term convergence to the full-field result.

Continuous measurement of numberlike observables has a strong effect on the conditional state of a quantum system, however, and it might be hoped that the *conditional* dynamics of a multimode quantum system might have different properties. Different modes undergoing number measurement do not necessarily collapse to number states if they also are being coupled through the Hamiltonian, so it is not clear *a priori* whether simulations of continuously measured systems are tractable. In this section, we demonstrate that the NPW method can, in fact, produce highly stable simulations of a multimode conditional quantum system. More specifically, we simulate a BEC undergoing a position measurement while being cooled as close to the ground state using active feedback to the trapping potential. This system has been of theoretical interest and has the potential for experimental demonstration [12–15]. It is governed by the following master equation:

$$d\hat{\rho} = (-i[\hat{H},\hat{\rho}] + \gamma \mathcal{D}[\hat{X}]\hat{\rho} + \gamma \mathcal{C}[\hat{X}]\hat{\rho})dt + \sqrt{\gamma}\mathcal{H}[\hat{X}]\hat{\rho} \circ dW. \tag{31}$$

This is a special case of Eq. (1) in Stratonovich form, where $\circ dW$ is a Stratonovich-Wiener increment; $\hat{X} = \int dx\, \hat{\psi}^\dagger(x) x \hat{\psi}(x)$ is the observable for a position measurement on a many-body system; the Hamiltonian for the trap is $\hat{H} = \int dx\, \hat{\psi}^\dagger(x) H(x) \hat{\psi}(x)$ with $H(x) = \frac{\omega}{2}(-\nabla_x^2 + x^2 + ux\langle \hat{P} \rangle / \langle \hat{N} \rangle)$ where $\hat{P} = \int dx\, \hat{\psi}^\dagger(x)(-i\nabla_x)\hat{\psi}(x)$ is a momentum for a many-body system, $\hat{N} = \int dx\, \hat{\psi}^\dagger(x)\hat{\psi}(x)$ is the total number, and $u = 1$ is the feedback parameter that controls the dampening we use to cool the system. This control was considered for a BEC without measurement in Ref. [49] under a mean-field approximation; it also has been solved optimally for a single-particle model in Ref. [12] with

simulations performed later in Ref. [13]. We now demonstrate a full-field simulation of this control.

An analytic solution or a direct integration of Eq. (31) is not possible, so we can only compare the evolution using the stochastic methods with approximate solutions. In the absence of interparticle interactions, the Hamiltonian and measurement are insensitive to the number statistics on the BEC, so we may expect the Hartree-Fock approximation to be appropriate [15]. The Hartree-Fock evolution can be integrated for long times, so although it requires stronger approximations, it can be used as a sanity check for simulations using the stochastic techniques. Including the traditional nonlinear terms in the Hamiltonian would be trivial for the NPW method, adding purely deterministic terms. We do not do this for the purposes of our demonstration because it would likely cause difficulties for our comparison methods. The Hartree-Fock approximation would be weaker in that regime and may converge to an incorrect result, and strong nonlinearities can prevent traditional stochastic methods from converging at all. Therefore, this simulation is a worst-case scenario for testing the NPW technique.

The Hartree-Fock approximation for the evolution (31) can be applied to the master equation (33) using the techniques analyzed in Ref. [15]. This gives the following stochastic partial-differential equation (SPDE):

$$d\alpha_H(x) = \{[-iH(x) - \gamma(x^2 - 2xX_1\mathbb{E}_H[X_1])]dt + \sqrt{\gamma}x \circ dW\}\alpha_H(x), \tag{32}$$

where $N = \int dx|\alpha_H(x)|^2$ is the norm. This is the unnormalized evolution of the Hartree-Fock wave equation. Observables are calculated using $\mathbb{E}_H[f(x)] = \int dx\, \alpha_H^*(x) f(x)\alpha_H(x)/N$. To improve efficiency of simulations, it must be normalized at each time step.

The first full-field simulation method we consider uses the TW representation. Using the techniques described in Refs. [18,19], we find the master equation (31) gives the following evolution for the functional Wigner distribution:

$$\begin{aligned} d\mathcal{W}[\boldsymbol{\alpha}] = \Bigg[& \int dx\{i\,\partial_{\alpha(x)}H(x) - i\,\partial_{\alpha^*(x)}H(x) + \gamma x\,\partial_{\alpha^*(x)}\partial_{\alpha(x)}(X_1 - \mathbb{E}_{\mathcal{W}}[X_1])\} + \gamma\int dx\int dy\, xy \\ & \times\left(-\frac{1}{2}\partial_{\alpha(x)}\partial_{\alpha(y)}\alpha(x)\alpha(y) + \partial_{\alpha^*(x)}\partial_{\alpha(y)}\alpha^*(x)\alpha(y) - \frac{1}{2}\partial_{\alpha^*(x)}\partial_{\alpha^*(y)}\alpha^*(x)\alpha^*(y) - \frac{1}{8}\partial_{\alpha^*(x)}\partial_{\alpha^*(y)}\partial_{\alpha(x)}\partial_{\alpha(y)}\right) \\ & + 2\gamma\left\{-X_1^2 + \mathbb{E}_{\mathcal{W}}\left[X_1^2\right] + 2(X_1 - \mathbb{E}_{\mathcal{W}}[X_1])\mathbb{E}_{\mathcal{W}}[X_1]\right\}\Bigg]dt + \left(-\frac{1}{2}\int dx\, x\,\partial_{\alpha^*(x)}\partial_{\alpha(x)} + 2\,(X_1 - \mathbb{E}_{\mathcal{W}}[X_1])\right)\circ dW, \end{aligned} \tag{33}$$

where $\mathbb{E}_{\mathcal{Q}}[f[\boldsymbol{\alpha}]] = \int d\mu(\boldsymbol{\alpha}) f[\boldsymbol{\alpha}]\mathcal{Q}[\boldsymbol{\alpha}]$ is our notation for integrating functional quasiprobability distributions $\mathcal{Q}$ over the functional measure $d\mu(\boldsymbol{\alpha})$ [24] and $X_1 = \int dx\, x|\alpha(x)|^2$ is the position moment. As in Sec. II, even after truncation, we are left with non-positive-semi-definite diffusion, and so, proceeding further would require a doubling of the phase space in a similar sense to the positive-P representation, and we will not pursue this approach.

Next, we consider the evolution of the positive-P representation. Once again, the master equation (31) can be unravelled using techniques from Refs. [18,19] to give the following evolution for the functional P distribution:

$$\begin{aligned} d\mathcal{P}[\boldsymbol{\alpha}] = \Bigg[& \Bigg(\int dx\,\partial_{\alpha(x)}\{iH(x) + \gamma[x^2 - 4x(X_1 + \mathbb{E}_{\mathcal{P}}[X_1])]\}\alpha(x) + \partial_{\alpha^*(x)}\{-iH(x) + \gamma[x^2 - 4x(X_1 + \mathbb{E}_{\mathcal{P}}[X_1])]\}\alpha^*(x) \\ & + \gamma\int dx\int dy\, xy[\partial_{\alpha^*(x)}\,\partial_{\alpha(y)}\alpha^*(x)\alpha(y)] + 2\gamma\left\{2(X_1 - \mathbb{E}_{\mathcal{P}}[X_1])\mathbb{E}_{\mathcal{P}}[X_1] - \left(X_2 + X_1^2 - \mathbb{E}_{\mathcal{P}}\left[X_2 + X_1^2\right]\right)\right\}\Bigg)dt \\ & + \sqrt{\gamma}\left(-\int dx\, x[\partial_{\alpha(x)}\alpha(x) + \partial_{\alpha^*(x)}\alpha^*(x)] + 2(X_1 - \mathbb{E}_{\mathcal{P}}[X_1])\right)\circ dW\Bigg]\mathcal{P}[\boldsymbol{\alpha}], \end{aligned} \tag{34}$$

where $X_2 = \int dx\, x^2|\alpha(x)|^2$. Equation (34) has non-positive-semi-definite diffusion and, as such, requires a doubling of the phase space. We, therefore, convert this evolution into the following set of SPDEs:

$$\begin{aligned} d\alpha_p(x) &= \{-i[H(x) + \sqrt{\gamma}x \circ (dV_1 + dV_2)] \\ &\quad + \sqrt{\gamma}\circ dW - 2\gamma x(X_1 - \mathbb{E}_f[X_1])dt\}\alpha_p(x), \\ d\alpha_p^+(x) &= \{i[H(x) + \sqrt{\gamma}x \circ (dV_1 - dV_2)] \\ &\quad + \sqrt{\gamma}\circ dW - 2\gamma x(X_1 - \mathbb{E}_f[X_1])dt\}\alpha_p^+(x) \\ d\omega_p &= \left\{-2\gamma\left(X_2 + X_1^2 - 2X_1\mathbb{E}_f[X_1]\right)dt \right. \\ &\quad \left. + 2\sqrt{\gamma}X_1 \circ dW\right\}\omega_p. \end{aligned} \tag{35}$$

The numerical solution of these equations is plotted in parts (b,i) and (b,ii) of Fig. 4 for a value of $\gamma/\omega = 0.01$. The doubling of the phase space makes the solution unstable, and they cannot be integrated past a thousandth of a trap period. The integration is stable in the limit of weak measurement, as demonstrated in Ref. [32] where the measurement strength was 6 orders of magnitude weaker. Realistic experiments typically require information to be acquired at a much faster rate, but these more realistic measurement strengths are not accessible with the positive-P representation methods.

We finally consider the full-field technique based on the NPW. All terms other than the kinetic-energy term can be simulated exactly, and the kinetic-energy term is approximated

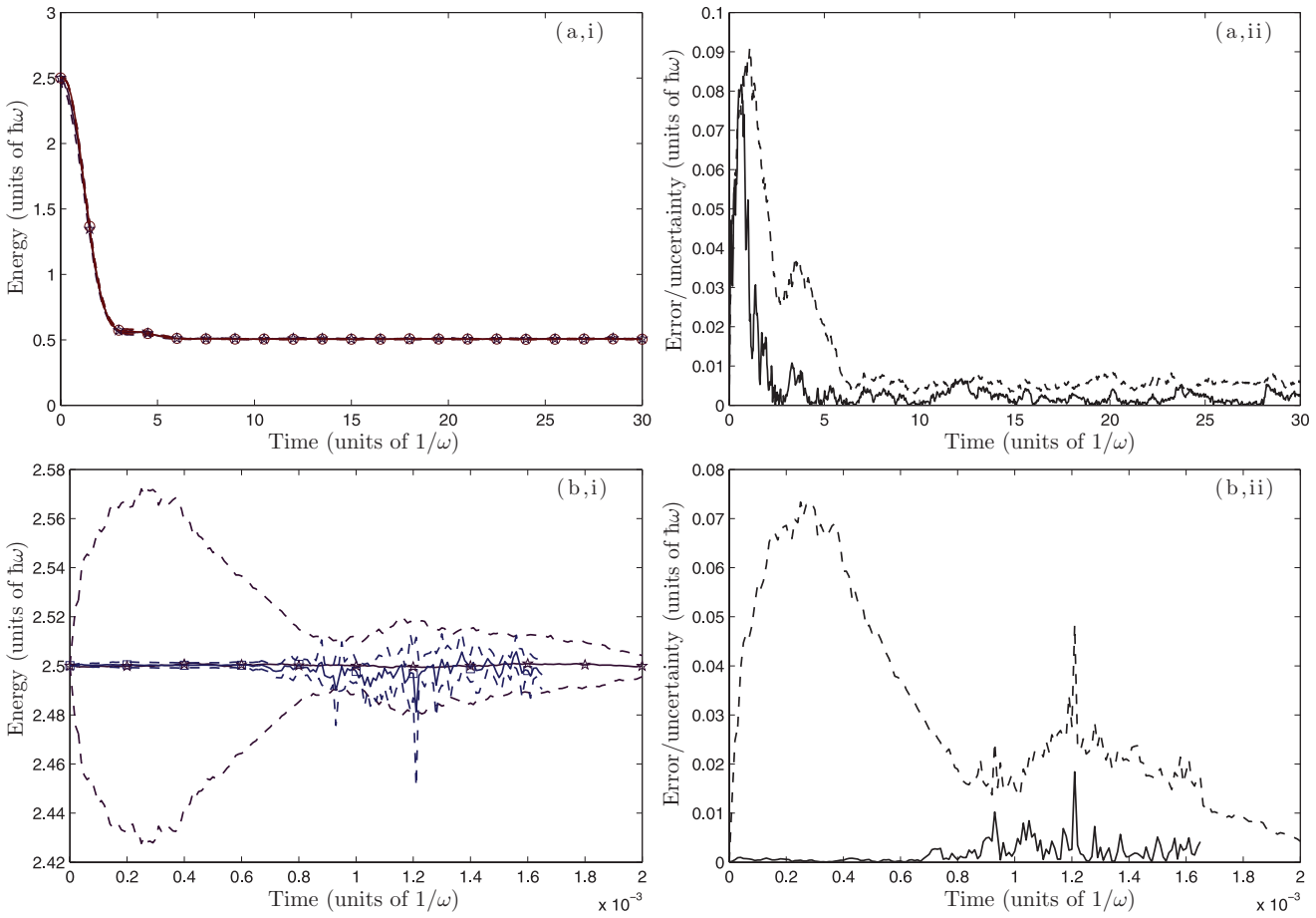

FIG. 4. (Color online) Comparison of the NPW (upper plots) and the positive-P representation (lower plots) methods for simulating a one-dimensional BEC undergoing continuous position measurement and feedback. All simulations use a value of $\gamma/\omega = 0.01$, $N = 10^4$, and an initial state of an offset Gaussian. The left-hand plots show the mean energy as a function of time for the stochastic simulations using the NPW [red circle in (a,i)] and the positive-P representations [blue squares in (b,i)]; both have a 2σ confidence interval plotted with dashed lines. The results for the numerical integration under the Hartree-Fock approximation are shown in both plots for comparison (purple stars, line). The positive-P representation results diverge after $t \approx 10^{-3}$ and are not plotted beyond this point. Plots (a,ii) and (b,ii) show, on a logarithmic scale, the difference between the stochastic result and the Hartree-Fock solution (solid black lines) and uncertainties in the stochastic result (dashed black line), corresponding to plots (a,i) and (b,i), respectively. The NPW simulation converges for at least 4 orders of magnitude longer than the positive-P representation.

as described in Sec. III A. The physical justification of the approximation is essentially the same as we find that the accuracy of the sampling increases with the total number N of the BEC. Special considerations need to be taken when sampling a BEC as opposed to a single mode, and these are discussed at the end of Appendix A. Using the results from Sec. III and the techniques in Ref. [29], we find the master equation (33) gives the following functional NPW distribution evolution:

$$\begin{aligned} d\mathcal{N}[\boldsymbol{\alpha}] = \Bigg[\Bigg(\int dx\, i\, \partial_{\alpha(x)} H(x)\alpha(x) - i\, \partial_{\alpha^*(x)} H(x)\alpha^*(x) \\ - 2\gamma \big\{ X_1^2 - \mathbb{E}_{\mathcal{N}}\big[X_1^2\big] \\ - 2(X_1 - \mathbb{E}_{\mathcal{N}}[X_1])\mathbb{E}_{\mathcal{N}}[X_1] \big\} \Bigg) dt \\ + 2\sqrt{\gamma}(X_1 - \mathbb{E}_{\mathcal{N}}[X_1]) \circ dW \Bigg] \mathcal{N}[\boldsymbol{\alpha}]. \end{aligned} \tag{36}$$

This is a valid FPE. Comparing to Eq. (33) or Eq. (34), we note that the form is much simpler and does not require a doubling of the phase space. We have performed a truncation in a similar sense to a traditional Wigner representation, which is valid in the large N limit. It is important to note this equation is now in Kushner-Stratonovich form [50,51], which is key to the comparative stability of the NPW method. We can unravel Eq. (36) into the following set of SPDEs:

$$\begin{aligned} d\alpha_n(x) &= -iH(x)\alpha_n(x), \\ d\omega_n &= \{-2\gamma(X_1^2 - 2X_1\mathbb{E}_f[X_1])dt + 2\sqrt{\gamma}X_1 \circ dW\}\omega_n. \end{aligned} \tag{37}$$

These equations were simulated and were plotted in parts (a,i) and (a,ii) of Fig. 4, which showed the energy as a function of time, and the difference between the Hartree-Fock approximate solution and the NPW technique, respectively. Part (a,ii) also shows the statistical uncertainty in the NPW solution, which is a sign of the convergence of the method.

Parameters used were $N = 10^4$ and $\gamma = 0.01\omega$. We can see that the NPW representation converges indefinitely and is shown to be consistent with the Hartree-Fock solution over a time scale at least 4 orders of magnitude larger than that of the the positive-P representation solution.

V. CONCLUSIONS

The paper showed that the NPW-based simulations were dramatically better than the simulations based on coherent-state representations for the conditional master equation (2), which described a system under a constant measurement of the form allowed in atom-optical systems. It also described approximations for simulating linear-coupling terms in multimode systems and showed that the NPW method was better than or equal to carefully adjusted TW methods for the two-mode Bose-Hubbard model. It then was shown that the NPW method can be applied successfully to produce a full quantum-field simulation of a multimode atom-optical system undergoing continuous measurement and feedback. The simulations were stable enough to consider long-term behavior of systems and to model the effects of feedback strategies. In particular, the method represented the only available option to model multimode experiments where approximations, such as Hartree-Fock or mean field fail. This high level of convergence can be explained by the suitability of the basis underlying the representation to the measurement eigenstates. Importantly, due to practical difficulties in producing stable atomic local oscillators, any current detection scheme used in quantum gases was of a form that was suited to the NPW method. The NPW method described in this paper was also the only simulation tool that was deterministic for the strong number-conserving nonlinearities that were present in such systems and, therefore, was the only suitable candidate for simulating conditional states of ultra-cold-atomic gases for feedback or state estimation.

ACKNOWLEDGMENTS

This research was supported under the Australian Research Council's Discovery Projects funding scheme (Project No. DP0556073) and the Australian Research Council Centre of Excellence for Quantum-Atom Optics (ACQAO). A.R.R.C. acknowledges support from the Australian Research Council Centre of Excellence for Quantum Computation and Communication Technology (Project No. CE110001027). Numerical integration was performed by using the open source software package XMDS [52]. We acknowledge the use of CPU time at the National Computational Infrastructure National Facility and thank Graham Dennis for his help with simulations.

APPENDIX A: SAMPLING OF A COHERENT STATE IN THE NPW METHOD

We approximate the distribution for a coherent state in the NPW representation to make it strictly positive by taking the large n limit. This ensures that the sampling of coherent states with the NPW method is scalable. To begin, we examine the original distribution of a coherent state in the NPW representation. By considering a coherent state with amplitude $\alpha_0 = \sqrt{n_0}e^{i\phi_0}$, using the correspondences given in Ref. [29], we get the following:

$$\mathcal{N}_{\alpha_0}(n,\phi) = \frac{1}{2\pi}\sum_{k=-n}^{n}\frac{n_0^n e^{2ik(\phi-\phi_0)-n_0}}{\sqrt{(n-k)!(n+k)!}}, \tag{A1}$$

where we should note n can take half-integer values $n = 0, \frac{1}{2}, 1, \frac{3}{2}, \ldots$. This function not only turns negative for certain values of n and ϕ, but also is in a form that is difficult to sample efficiently. We want to both restore positivity and convert it to a form that can be sampled efficiently. We begin by approximating the square-root factorial expression using a Taylor expansion about $k = 0$,

$$-\ln[\sqrt{(n-k)!(n+k)!}] = -\ln(n!) - \frac{1}{2}\psi^{(1)}(n+1)k^2 + O(k^4), \tag{A2}$$

where $\psi^{(1)}(n+1)$ is the trigamma function. Truncating the k^4 order and above, which is valid in the large n limit, we find

$$\mathcal{N}_{\alpha_0}(n,\phi) = \frac{n_0^n e^{-n_0}}{n!}\frac{1}{2\pi}\sum_{k=-\infty}^{\infty} \times \exp\left[\frac{1}{2}\psi^{(1)}(n+1)k^2 + 2ik(\phi-\psi)\right], \tag{A3}$$

where we also have taken the sum limits to infinity as the Gaussian function is approximately zero for k large. This is a Fourier series, which we can evaluate analytically and reduces our expression to

$$\mathcal{N}_{\alpha_0}(n,\phi) = \frac{n_0^n e^{-n_0}}{n!}\left(\frac{\exp\left[\frac{-2(\phi-\phi_0)^2}{\psi^{(1)}(n+1)}\right]}{\sqrt{2\pi\,\psi^{(1)}(n+1)}} + \frac{(-1)^{2n}\exp\left\{\frac{-2[\phi-(\phi_0+\pi)]^2}{\psi^{(1)}(n+1)}\right\}}{\sqrt{2\pi\,\psi^{(1)}(n+1)}}\right). \tag{A4}$$

We now have a manageable analytic expression for the NPW distribution. But we still have negativity present. Specifically, the negativity occurs when n is a half integer. As we performed in Sec. III A where we considered the large n limit and approximated $n + \frac{1}{2} \approx n$, we can sum the integer and half-integer terms together to get the following expression:

$$\mathcal{N}_{\alpha_0}(n,\phi) = \frac{n_0^n \exp\left(-n_0 + \frac{-2(\phi-\phi_0)^2}{\psi^{(1)}(n+1)}\right)\sqrt{2}}{n!\sqrt{\pi\,\psi^{(1)}(n+1)}}, \tag{A5}$$

where n is now an integer. We could have taken n to the continuum limit at an earlier stage, but by retaining the integer aspect of n for the sampling stage, we are performing a weaker approximation and can reproduce the results presented in Ref. [29]. Now, the distribution strictly is positive, allowing for scalable sampling. The coherent state appears in the analysis of many quantum systems making this result crucial for the success of the NPW representation. We also note the distribution is in a convenient analytic form. Algorithmically, in order to sample this distribution, first sample a Poisson distribution with mean n_0 to give a stochastic variable for n. Then, sample a Gaussian variable with mean ϕ_0 and variance $\frac{1}{4}\psi^{(1)}(n+1)$ to get the stochastic variable for ϕ.

This result is particularly useful when sampling BEC states, which typically are expressible as a product of coherent states that have an arbitrary total phase. The wave function of a BEC is normally in a basis that has a small amplitude in some of the modes. Initially, it may seem that this would break the large n limit requirement. However, we found that this approximation works well for most BEC distributions with a total number as small as 1000. This was contingent on a minor modification to the algorithm already proposed. To begin, sample a Poisson distribution with mean n_0 to give a stochastic variable for n. If $n=0$, a special case occurs where ϕ is sampled from a uniform distribution over the interval $[0,2\pi)$. If $n\neq 0$, then the algorithm continues per usual, and ϕ is sampled by a Gaussian variable with mean ϕ_0 and variance $\frac{1}{4}\psi^{(1)}(n+1)$.

The need for this special case can be understood as follows. The approximations we use becomes less accurate for small n; this only becomes a serious consideration for the $n=0$ case. Physically, the $n=0$ case is a sample of a vacuum state. However, we note that $\mathcal{N}_{\alpha_0}(0,\phi)$ is not a uniform distribution. This is a contradiction as the vacuum must not have any phase information. Thus, when $n=0$, a uniform distribution is used instead. Also, sampling $n=1$ would not necessarily be exact, but in practice, it is sufficient to only treat $n=0$ as a special case.

APPENDIX B: DERIVATION OF THE MULTIMODE FPE

In this section, our aim is to complete the steps necessary to find the conditional FPE for the NPW representation derived from the master equation (31). The nonlinearity, decoherence, and conditioning terms in the master equation are all immediately in Fokker-Planck form when using the NPW. Thus, we primarily are concerned with the Hamiltonian, which produces terms that must be approximated. We have commented on the physical validity of the approximations in Sec. III. This extension to the multimode case is simply the application of those approximations for arbitrary numbers of modes, and we present it for completeness.

To begin, we consider the Hamiltonian term from the master equation (31),

$$\partial_t\hat{\rho} = -i\left[\int dx\ \hat{\psi}^\dagger(x)H(x)\hat{\psi}(x),\hat{\rho}\right]. \tag{B1}$$

We convert it into a countably infinite basis such that $\int dx\ \hat{\psi}^\dagger(x)H(x)\hat{\psi}(x) = \sum_{ij}\hat{a}_i^\dagger H_{ij}\hat{a}_j$, where $\hat{\psi}(x) = \sum_i u_i(x)\hat{a}_i$ and $u_i(x)$ is a square-integrable orthonormal set of basis functions and H_{ij} are the coefficients of a Hermitian matrix. The Hamiltonian evolution can now be written as

$$\partial_t\hat{\rho} = -i\left[\sum_i H_{ii}\hat{a}_i^\dagger\hat{a}_i + \sum_{i<j}(H_{ij}\hat{a}_i^\dagger\hat{a}_j + H_{ij}^*\hat{a}_j^\dagger\hat{a}_i),\hat{\rho}\right]. \tag{B2}$$

In this more illuminating form, we can see, from the work in Sec. III A, that this produces the following conditional Fokker-Planck evolution using the NPW representation:

$$\begin{aligned}\partial_t\mathcal{N}[\boldsymbol{n},\boldsymbol{\phi}] = \Bigg[&\sum_i \partial_{\phi_i}H_{ii} + \sum_{i<j}\Bigg(2i(\partial_{n_j}-\partial_{n_i})\\ &\times\sqrt{\left(n_i+\frac{1}{2}\right)\left(n_j+\frac{1}{2}\right)}\\ &\times(H_{ij}^*e^{-i(\phi_j-\phi_i)} - H_{ij}e^{i(\phi_j-\phi_i)})\\ &+\frac{1}{2}\left(\partial_{\phi_i}\frac{\sqrt{n_j+\frac{1}{2}}}{\sqrt{n_i+\frac{1}{2}}} + \partial_{\phi_j}\frac{\sqrt{n_i+\frac{1}{2}}}{\sqrt{n_j+\frac{1}{2}}}\right)\\ &\times(H_{ij}e^{i(\phi_j-\phi_i)} + H_{ij}^*e^{-i(\phi_j-\phi_i)})\Bigg)\Bigg]\\ &\times\mathcal{N}[\boldsymbol{n},\boldsymbol{\phi}].\end{aligned} \tag{B3}$$

We can apply a similar transformation that was used to produce Eq. (20), and we can let $\alpha_k \approx \sqrt{n_k+\frac{1}{2}}e^{i\phi_k}$. This changes the conditional FPE to

$$\partial_t\mathcal{N}[\boldsymbol{n},\boldsymbol{\phi}] = \left(\sum_{i,j} i\ \partial_{\alpha_i}H_{ij}\alpha_j - i\ \partial_{\alpha_i^*}H_{ij}^*\alpha_j^*\right)\mathcal{N}[\boldsymbol{n},\boldsymbol{\phi}]. \tag{B4}$$

We can transform this back into the position basis to give

$$d\mathcal{N}[\boldsymbol{n},\boldsymbol{\phi}] = [i\ \partial_{\alpha(x)}H(x)\alpha(x) - i\ \partial_{\alpha^*(x)}H(x)\alpha^*(x)]\mathcal{N}[\boldsymbol{n},\boldsymbol{\phi}], \tag{B5}$$

where $\alpha(x)=\sum_i u_i(x)\alpha_i$. Equation (B5) is now in Fokker-Planck form. The decoherence and conditioning terms are all straightforward and do not require any approximation. Using this result, we immediately can derive the result presented in Eq. (33).

[1] V. Giovannetti, S. Lloyd, and L. Maccone, Phys. Rev. Lett. **96**, 010401 (2006).

[2] D. Leibfried, M. D. Barrett, T. Schaetz, J. Britton, J. Chiaverini, W. M. Itano, J. D. Jost, C. Langer, and D. J. Wineland, Science **304**, 1476 (2004).

[3] M. A. Nielsen and I. Chuang, *Quantum Computation and Quantum Information* (Cambridge University Press, Cambridge, UK, 2000).

[4] N. Gisin, G. Ribordy, W. Tittel, and H. Zbinden, Rev. Mod. Phys. **74**, 145 (2002).

[5] H. Mabuchi and A. C. Doherty, Science **298**, 1372 (2002).
[6] A. C. Doherty, S. Habib, K. Jacobs, H. Mabuchi, and S. M. Tan, Phys. Rev. A **62**, 012105 (2000).
[7] D. A. Steck, K. Jacobs, H. Mabuchi, T. Bhattacharya, and S. Habib, Phys. Rev. Lett. **92**, 223004 (2004).
[8] W. P. Smith, J. E. Reiner, L. A. Orozco, S. Kuhr, and H. M. Wiseman, Phys. Rev. Lett. **89**, 133601 (2002).
[9] V. Belavkin, Automat. Remote Contr. **44**, 178 (1983).
[10] H. M. Wiseman and G. J. Milburn, Phys. Rev. Lett. **70**, 548 (1993).
[11] J. K. S. Ramon van Handel and H. Mabuchi, J. Opt. B **7**, S179 (2005).
[12] A. C. Doherty and K. Jacobs, Phys. Rev. A **60**, 2700 (1999).
[13] S. D. Wilson, A. R. R. Carvalho, J. J. Hope, and M. R. James, Phys. Rev. A **76**, 013610 (2007).
[14] S. S. Szigeti, M. R. Hush, A. R. R. Carvalho, and J. J. Hope, Phys. Rev. A **80**, 013614 (2009).
[15] S. S. Szigeti, M. R. Hush, A. R. R. Carvalho, and J. J. Hope, Phys. Rev. A **82**, 043632 (2010).
[16] H. M. Wiseman and G. J. Milburn, *Quantum Measurement and Control* (Cambridge University Press, Cambridge, UK, 2010).
[17] H. M. Wiseman and L. K. Thomsen, Phys. Rev. Lett. **86**, 1143 (2001).
[18] C. Gardiner, *Handbook of Stochastic Methods for Physics, Chemistry, and Natural Sciences* (Springer-Verlag, Berlin, 1983).
[19] C. Gardiner and P. Zoller, *Quantum Noise: A Handbook of Markovian and non-Markovian Quantum Stochastic Methods with Applications to Quantum Optics* (Springer-Verlag, Berlin, 2000).
[20] P. D. Drummond and S. J. Carter, J. Opt. Soc. Am. B **4**, 1565 (1987).
[21] P. D. Drummond and J. F. Corney, Phys. Rev. A **60**, R2661 (1999).
[22] J. J. Hope, Phys. Rev. A **64**, 053608 (2001).
[23] J. F. Corney and P. D. Drummond, Phys. Rev. Lett. **93**, 260401 (2004).
[24] M. J. Steel, M. K. Olsen, L. I. Plimak, P. D. Drummond, S. M. Tan, M. J. Collett, D. F. Walls, and R. Graham, Phys. Rev. A **58**, 4824 (1998).
[25] R. G. Dall, L. J. Byron, A. G. Truscott, G. R. Dennis, M. T. Johnsson, and J. J. Hope, Phys. Rev. A **79**, 011601 (2009).
[26] C. M. Savage and K. V. Kheruntsyan, Phys. Rev. Lett. **99**, 220404 (2007).
[27] A. Gilchrist, C. W. Gardiner, and P. D. Drummond, Phys. Rev. A **55**, 3014 (1997).
[28] A. Sinatra, C. Lobo, and Y. Castin, J. Phys. B **35**, 3599 (2002).
[29] M. R. Hush, A. R. R. Carvalho, and J. J. Hope, Phys. Rev. A **81**, 033852 (2010).
[30] K. Jacobs, L. Tian, and J. Finn, Phys. Rev. Lett. **102**, 057208 (2009).
[31] A. R. R. Carvalho and M. F. Santos, New J. Phys. **13**, 013010 (2011).
[32] M. R. Hush, A. R. R. Carvalho, and J. J. Hope, Phys. Rev. A **80**, 013606 (2009).
[33] D. A. R. Dalvit, J. Dziarmaga, and R. Onofrio, Phys. Rev. A **65**, 053604 (2002).
[34] L. K. Thomsen and H. M. Wiseman, Phys. Rev. A **65**, 063607 (2002).
[35] J. Ruostekoski and D. F. Walls, Phys. Rev. A **56**, 2996 (1997).
[36] J. F. Corney and G. J. Milburn, Phys. Rev. A **58**, 2399 (1998).
[37] C.-F. Li and G.-C. Guo, Phys. Lett. A **248**, 117 (1998).
[38] U. Leonhardt, T. Kiss, and P. Piwnicki, Eur. Phys. J. D **7**, 413 (1999).
[39] Y. Korennoy and V. Man'ko, J. Russ. Laser Res. **32**, 74 (2011).
[40] M. R. Andrews, C. G. Townsend, H.-J. Miesner, D. S. Durfee, D. M. Kurn, and W. Ketterle, Science **275**, 637 (1997).
[41] T. Esslinger, I. Bloch, and T. W. Hänsch, Phys. Rev. A **58**, R2664 (1998).
[42] P. Öhberg and S. Stenholm, Phys. Rev. A **57**, 1272 (1998).
[43] G. J. Milburn, J. Corney, E. M. Wright, and D. F. Walls, Phys. Rev. A **55**, 4318 (1997).
[44] R. Franzosi and V. Penna, Phys. Rev. A **63**, 043609 (2001).
[45] We also could have kept n quantized and could have tried to change the expression above to a Poissonian jump process with strictly positive jump probabilities. However, the order of convergence of this approach would be no better than the continuum limit we have used in Eq. (15). The continuum limit also has the advantage that its simulations involve deterministic evolution, which is considerably easier to implement than jump-based evolution.
[46] M. Olsen and A. Bradley, Opt. Commun. **282**, 3924 (2009).
[47] C. W. Gardiner, J. R. Anglin, and T. I. A. Fudge, J. Phys. B **35**, 1555 (2002).
[48] M. Olsen, L. Plimak, S. Rebic, and A. Bradley, Opt. Commun. **254**, 271 (2005).
[49] S. A. Haine, A. J. Ferris, J. D. Close, and J. J. Hope, Phys. Rev. A **69**, 013605 (2004).
[50] R. L. Stratonovich, Theory Probab. Appl. **5**, 156 (1960).
[51] H. J. Kushner, J. Math. Anal. Appl. **8**, 332 (1964).
[52] Project website [http://www.xmds.org].